ACS OMEGA

http://pubs.acs.org/journal/acsodf

Article

Trace Analysis of Emerging Virus: An Ultrasensitive ECL-Scan Imaging System for Viral Infectious Disease

Yunxia Wu,[#] Ronghua Yang,[#] Qikang Wu,[#] Mingxing Huang,[#] Bowen Shu, Wenjie Wu, Baoqing Sun,* Jinyu Xia,* Xiaodong Chen,* and Yuhui Liao*

Cite This: *ACS Omega* 2022, 7, 37499−37508

Read Online

ACCESS | Metrics & More | Article Recommendations | Supporting Information

ABSTRACT: Emerging infectious diseases have brought a huge impact on human society in recent years. The outbreak of Zika virus (ZIKV) in the Americas resulted in a large number of babies born with microcephaly. More seriously, the Coronavirus Disease 2019 (COVID-19) was globally spread and caused immeasurable damages. Thus, the monitoring of highly pathogenic viruses is important to prevent and control emerging infectious diseases. Herein, a dendritic polymer probe-amplified ECL-scan imaging system was constructed to realize trace analysis of viral emerging infectious diseases. A dendritic polymer probe was employed as the efficient signal emitter component that could generate an amplified ECL signal on the integrated chip, and the signal was detected by a single-photon level charge coupled device-based ECL-scan imaging system. With this strategy, the ZIKV in a complex system of blood, urine, and saliva was detected. The results indicated that a high sensitivity of 50 copies and superior specificity were achieved. Furthermore, this strategy realized highly sensitive detection (10 copies) of the S and N protein gene sequence of the Severe Acute Respiratory Syndrome Coronavirus 2 (SARS-Cov2) and spiked pseudovirus samples. Thus, the dendritic polymer probe-amplified ECL-scan imaging system suitably met the strict clinical requirements for trace analysis of an emerging virus, and thus has the potential to serve as a paradigm for monitoring emerging infectious diseases.

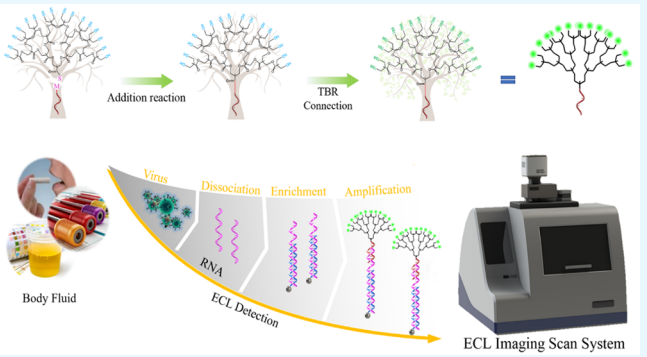

INTRODUCTION

With the development of economic globalization, the population density and mobility have greatly increased in recent years. The accompanying problem is the safety, prevention, and control of highly pathogenic microorganisms. In 2015, the Zika virus (ZIKV),[1−3] an *Aedes* mosquito-borne flavivirus,[4,5] was widespread in the Americas[6−8] and was declared as a Public Health Emergency of International Concern by World Health Organization (WHO).[9−11] ZIKV spreads in a variety of ways, including by infected mosquito bite.[12,13] It also can be transmitted by mother-to-fetus transmission,[14] sexual contact,[15,16] or blood transfusion.[17] Meanwhile, it has been proven that ZIKV infection was a main cause of Guillain-Barre syndrome,[18,19] congenital microcephaly,[20] and neurological defects in newborns.[21] Also ZIKV caused huge economic losses and health threats in the Americas. Fortunately, the ZIKV did not induce global spread.

More seriously, the Coronavirus Disease 2019 (COVID-19)[22,23] was spread globally and caused immeasurable damages. The infection of Severe Acute Respiratory Syndrome Coronavirus 2 (SARS-Cov2)[24,25] could cause the clinical symptoms of fever, chest pain, chills, rapid heartbeat, breathing difficulties, pneumonia, and kidney failure.[26−33] More than 250 million patients were confirmed to be infected with SARS-Cov2, which could spread though droplet transmission induced by coughing, sneezing, and touch, and the virus caused 5.1 million deaths (according to the statistics of Johns Hopkins university until Nov-16-2021). The mortality due to this virus is more than 10% in some European countries such as France,[34,35] England,[36] and Italy,[37,38] and the SARS-Cov2 has brought unprecedented influence on human society. However, biomedical analysis and accurate diagnosis of a viral emerging infectious disease are still unreliable because infected patients can be asymptomatic or present symptoms like other febrile illnesses. Thus, the monitoring of highly pathogenic virus is of great significance to the prevention and control of emerging infectious disease.

Electrochemiluminescence (ECL) is a versatile and powerful analytical technique, and since the first ECL reactions were

Received: July 7, 2022
Accepted: October 4, 2022
Published: October 14, 2022

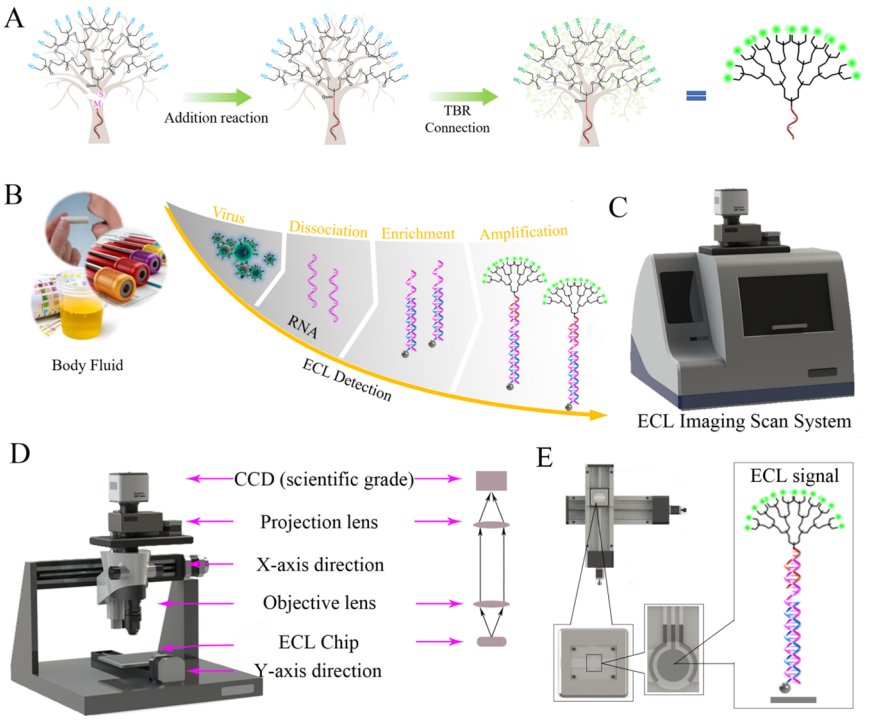

Figure 1. Design of dendritic $Ru(bpy)_3^{2+}$-polymer amplified ECL-scan imaging system. (A) Formation process of dendritic polymer probe. (B) ECL detection process of dendritic $Ru(bpy)_3^{2+}$-polymer amplified ECL-scan imaging system. (C) Structure of ECL-scan imaging system. (D) Structure of ECL-scan imaging system. (E) Details of ECL chip.

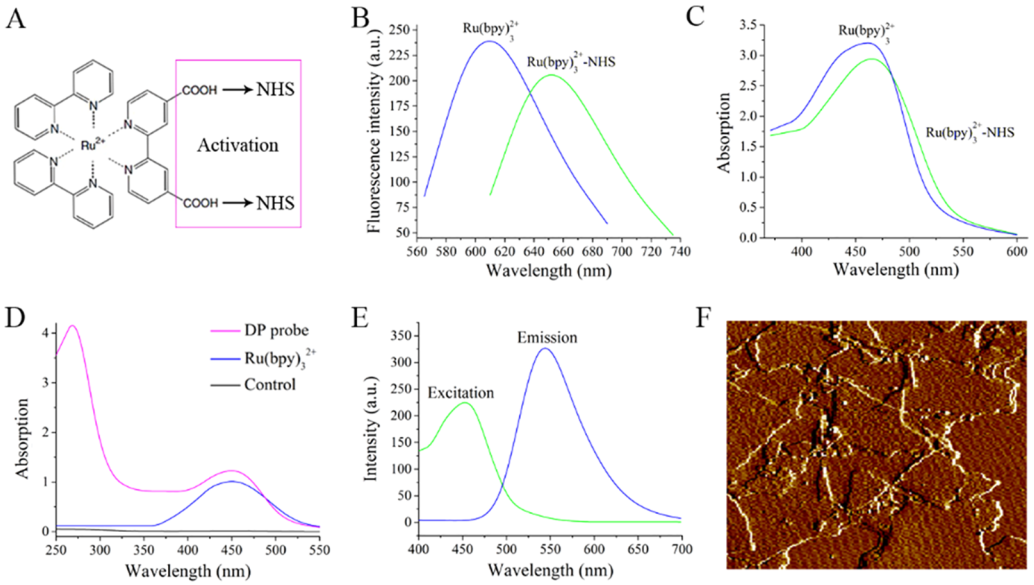

Figure 2. Characterization of dendritic $Ru(bpy)_3^{2+}$-polymer. (A) Molecular structure and activation process of $Ru(bpy)_3^{2+}$. (B) Fluorescence characterization of $Ru(bpy)_3^{2+}$ and the activated $Ru(bpy)_3^{2+}$. (C) Absorption characterization of $Ru(bpy)_3^{2+}$ and the activated $Ru(bpy)_3^{2+}$. (D) Absorption characterization of dendritic $Ru(bpy)_3^{2+}$-polymer probe. (E) Excitation and emission of dendritic $Ru(bpy)_3^{2+}$-polymer probe. (F) Morphology of dendritic $Ru(bpy)_3^{2+}$-polymer probe under atomic force microscope (AFM).

reported in the 1960s,[39,40] ECL has been widely applied in various fields, including biological clinical and applications.[41] ECL is mainly a luminescence process caused by the relaxation of electronically excited products to the ground state after an electrochemical reaction, including an electrochemical excitation step and a photoemission process. Specifically, the electrochemical reaction provides the active intermediate and the excited state photophore; in the subsequent luminescence relaxation process, the excited photophore returns to the ground state and emits an ECL signal.[42] Compared to other optical-based analysis methods, ECL has the following advantages. First, no external light source is required, and background noise from autofluorescence or scattered light is completely avoided. Second, the potential applied to the electrode allows for controlled ECL signal release. Third, the method has a fast response, high sensitivity, wide detection range, and low cost, and only small instruments are required.[43−46]

https://doi.org/10.1021/acsomega.2c04280
ACS Omega 2022, 7, 37499−37508

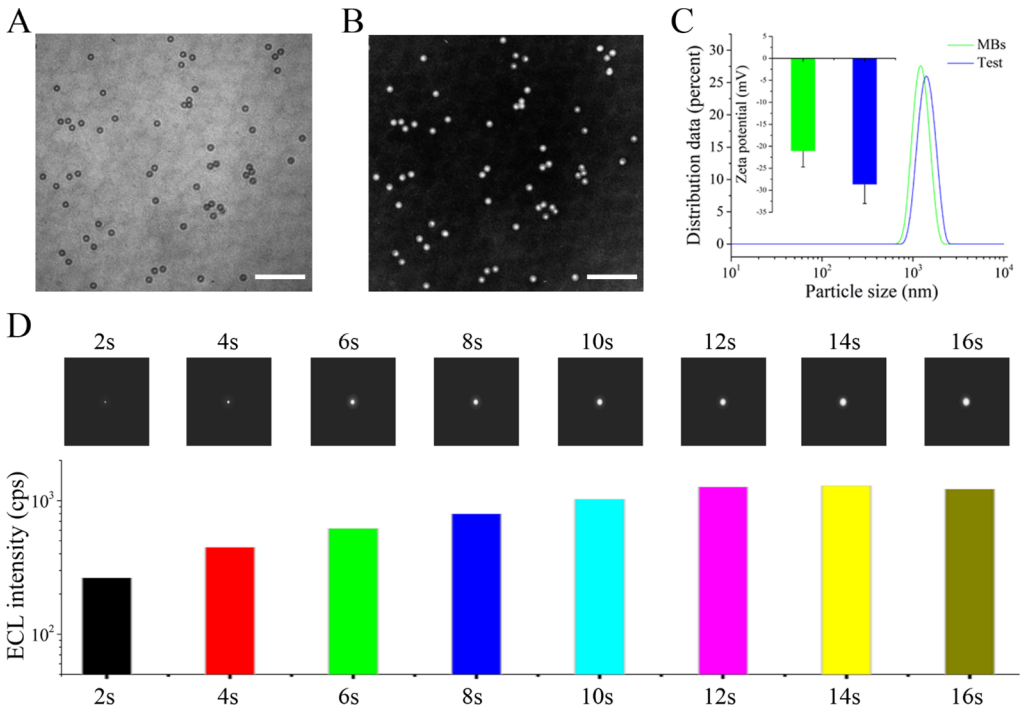

Figure 3. Principle validation of dendritic $Ru(bpy)_3^{2+}$-polymer amplified ECL-scan imaging system. (A) ECL generation complex with streptavidin-labeled magnetic beads under light field. Scale bar: 10 μm. (B) ECL signal detection of ECL generation complex under dark field. Scale bar: 10 μm. (C) Particle size and zeta potential of streptavidin-labeled magnetic beads and ECL generation complex with streptavidin-labeled magnetic beads. (D) Optimization of the time of data acquisition.

Herein, a dendritic polymer probe-amplified ECL-scan imaging system was constructed to realize trace analysis of viral emerging infectious disease (Figure 1). The dendritic polymer probe was employed as the efficient signal emitter component that could generate an amplified ECL signal on the integrated chip, and the signal was detected by a single-photon level charge coupled device-based ECL-scan imaging system. With this strategy, the ZIKV in the complex system of blood, urine, and saliva was detected. The results indicated that a high sensitivity of 10 copies and superior specificity were achieved. Furthermore, this strategy simultaneously realized ultrasensitive detection of the S and N protein gene of the SARS-Cov2 and spiked pseudovirus samples. Therefore, the dendritic polymer probe-amplified ECL-scan imaging system suitably met the strict clinical requirements for trace analysis of a highly pathogenic virus, and thus has the potential to be a new paradigm for emerging infectious diseases.

RESULTS AND DISCUSSION

Design of Dendritic $Ru(bpy)_3^{2+}$-Polymer Amplified ECL-Scan Imaging System. The dendritic $Ru(bpy)_3^{2+}$-polymer amplified ECL-scan imaging system was constructed for trace analysis of viral emerging infectious diseases. In this strategy, the dendritic polymer probe was used as a component that could generate an amplified ECL signal on an integrated chip. The formation process of the dendritic polymer probe is shown in Figure 1A. The dendritic polymer was connected to a DNA recognition domain by the addition reaction of a sulfydryl double bond, and the detailed process is shown in Figure S1. Then, the ECL luminophore of $Ru(bpy)_3^{2+}$ was linked to the dendritic polymer that could generate an intense ECL signal. The virus sample was dissociated to release RNA which was immobilized by capture probe (Figure 1B), and the dendritic polymer probe was subsequently added to form the complete ECL generation complex with streptavidin-labeled magnetic beads. The ECL signal was definitively detected by a single-photon level charge coupled device-based ECL-scan imaging system. The structure of the ECL-scan imaging system and the ECL chip are shown in Figure 1C,D. With this strategy, the ZIKV in the complex system of blood, urine, and saliva was detected. Furthermore, this strategy simultaneously realized highly sensitive detection of the S protein gene sequence of SARS-Cov2 and spiked samples.

Characterization of Dendritic $Ru(bpy)_3^{2+}$-Polymer. The molecular structure and the activation process of $Ru(bpy)_3^{2+}$ are shown in Figure 2A. $Ru(bpy)_3^{2+}$ was synthesized following the protocol in our previously published works,[47,4849] and the synthetic route is listed in Figure S2. The fluorescence and absorption characterization in Figure 2B,C indicated that the synthesis of $Ru(bpy)_3^{2+}$ and the activation were feasible, and the results were consistent with previous results. Then, we verified the connection between the dendritic $Ru(bpy)_3^{2+}$-polymer and the DNA recognition domain. The results in Figure 2D,E confirmed the feasibility of the connection between the dendritic $Ru(bpy)_3^{2+}$-polymer and the DNA recognition domain. The AFM results in Figure 2F showed that the morphology of the dendritic $Ru(bpy)_3^{2+}$-polymer probe appeared to be an irregular sheet distribution. The above characterization results proved the feasibility of dendritic $Ru(bpy)_3^{2+}$-polymer probe. Meanwhile, the stability of the dendritic $Ru(bpy)_3^{2+}$-polymer probe was investigated. The results in Figures S3, S4, S5, and S6 indicated that the dendritic $Ru(bpy)_3^{2+}$-polymer probe could remain stable at the high temperature of 95 °C, at the pH in the range of 5.0−8.5, in different buffers (PBS, SSC, and Tris-HCl), and in the complex biosystem of blood, urine, and saliva.

https://doi.org/10.1021/acsomega.2c04280
ACS Omega 2022, 7, 37499−37508

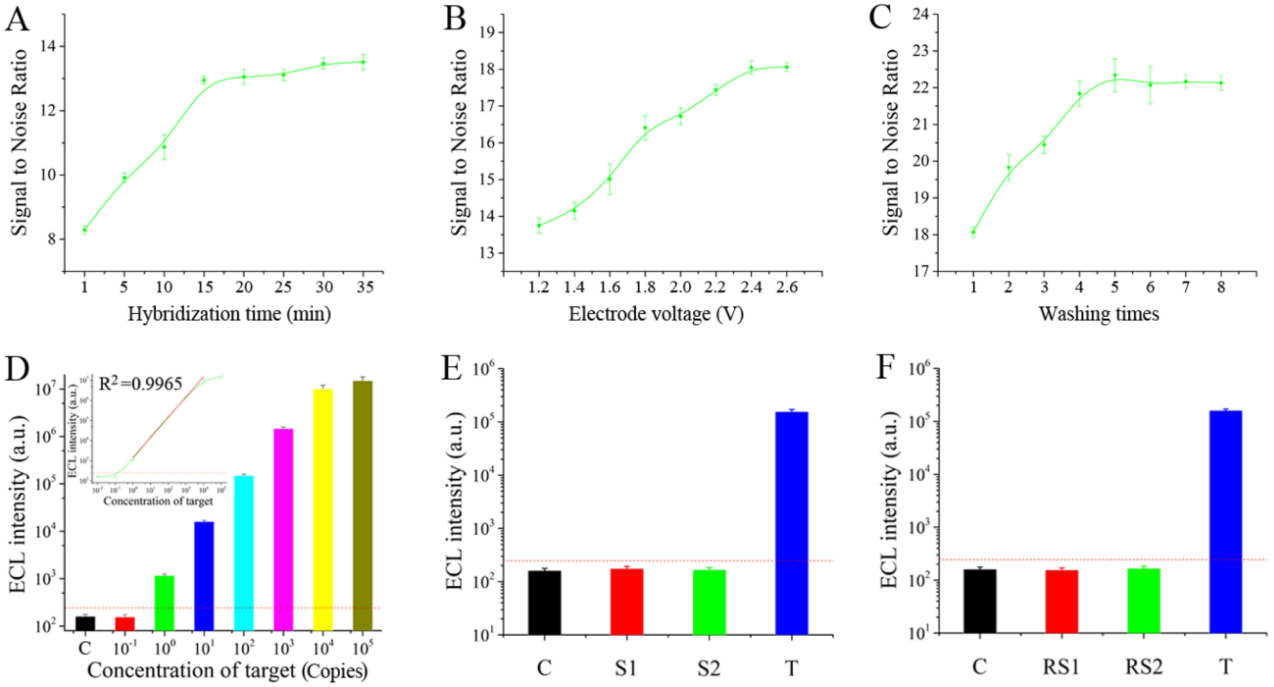

Figure 4. Optimization, sensitivity, and specificity of dendritic $Ru(bpy)_3^{2+}$-polymer amplified ECL-scan imaging system. (A). Optimization of hybridization time. (B) Optimization of electrode voltage. (C) Optimization of washing time. (D) Sensitivity and linear analysis of dendritic $Ru(bpy)_3^{2+}$-polymer amplified ECL-scan imaging system. (E) Specificity of dendritic $Ru(bpy)_3^{2+}$-polymer amplified ECL-scan imaging system with S1 and S2. (F) Specificity of dendritic $Ru(bpy)_3^{2+}$-polymer amplified ECL-scan imaging system with random sequence of RS1 and RS2.

Principle Validation, Optimization, and Sensitivity of ECL-Scan Imaging System. The ECL-scan imaging system comprised the single-photon level charge coupled device, the microscope system, and the ECL system. The ECL signal that was generated by the dendritic $Ru(bpy)_3^{2+}$-polymer probe was actuated by the ECL system, which was comprised the ECL chip and the high-precision motorized positioning systems (*X* and *Y* axis direction). The ECL signal was first focused by the objective lens and projection lens of the microscope, and then collected by the single-photon level charge coupled device. Under the light field, the complete ECL detection complex with streptavidin-labeled magnetic beads emerged as a spherical morphology (Figure 3A). While the electric field was added, the ECL signal was generated on the ECL chip and detected by the single-photon level charge coupled device under the dark field. The results in Figure 3B showed that intense ECL signal was generated on the surface of streptavidin-labeled magnetic beads. The particle size and zeta potential of streptavidin-labeled magnetic beads showed obvious distinction after the target was present (Figure 3C). The time (exposure time of the ECL-scan imaging system) of data acquisition was optimized. The results in Figure 3D indicated that the ECL intensity increased with the extension of time, and reached a plateau at the time point of 12 s, which means at this time point, the sensitivity of the ECL system is the highest, and the detection time is the shortest. Therefore, we select 12 s as the optimal time of data acquisition. Furthermore, the key factors of experiment were evaluated in Figure 4A,B,C. The results indicated that the optimal experiment conditions of hybridization time, electrode voltage, and washing time were set as 15 min, 2.4 V, and 4 times.

With the optimal experiment conditions, we evaluated the sensitivity of dendritic $Ru(bpy)_3^{2+}$-polymer amplified ECL-scan imaging system with the sequence from the HBsAg gene of the Hepatitis B virus (HBV). The sequence was listed in Table S1. The results in Figure 4D revealed that the dendric $Ru(bpy)_3^{2+}$-polymer probe reached a high sensitivity of 1 fmol, and provided a wide linear response range from 1 fmol to 10^4 fmol. Therefore, the excellent luminescence of the dendric $Ru(bpy)_3^{2+}$-polymer probe provided the foundation for clinical detection and diagnosis. Furthermore, we investigated the specificity of dendric $Ru(bpy)_3^{2+}$-polymer probe by comparing the ECL intensity between the specific sequence and random sequences. The sequence was listed in Table S1. The results in Figure 4E,F indicated that only the specific HBV sequence resulted in intense ECL; random sequences showed essentially the same ECL intensity as that of the control group. This result verifies the specificity of the dendric $Ru(bpy)_3^{2+}$-polymer probe.

Application of Dendritic $Ru(bpy)_3^{2+}$-Polymer Amplified ECL-Scan Imaging System for Zika Virus. Zika virus (ZIKV), an *Aedes* mosquito-borne flavivirus, was widespread in the Americas in 2015. It was declared as a Public Health Emergency of International Concern by World Health Organization (WHO) and caused huge economic losses and health threats in the Americas. Herein, we expanded the application of dendritic $Ru(bpy)_3^{2+}$-polymer amplified ECL-scan imaging system for detection of ZIKV. The conserved sequence from the ZIKV *NS1* gene was designed, and the genomes of the ZIKV strains and the other flaviviruses used in the present study were downloaded from the National Center for Biotechnology Information (NCBI) database (http://www.ncbi.nlm.nih.gov/genome/viruses/variation/Zika/), and aligned with the analysis software of MEGA 7. Conserved ZIKV-specific sequences that were divergent from other flaviviruses were identified. The sequence of ZIKV and other flavivirus strains, sequence of capture probe and signal probe

https://doi.org/10.1021/acsomega.2c04280
ACS Omega 2022, 7, 37499−37508

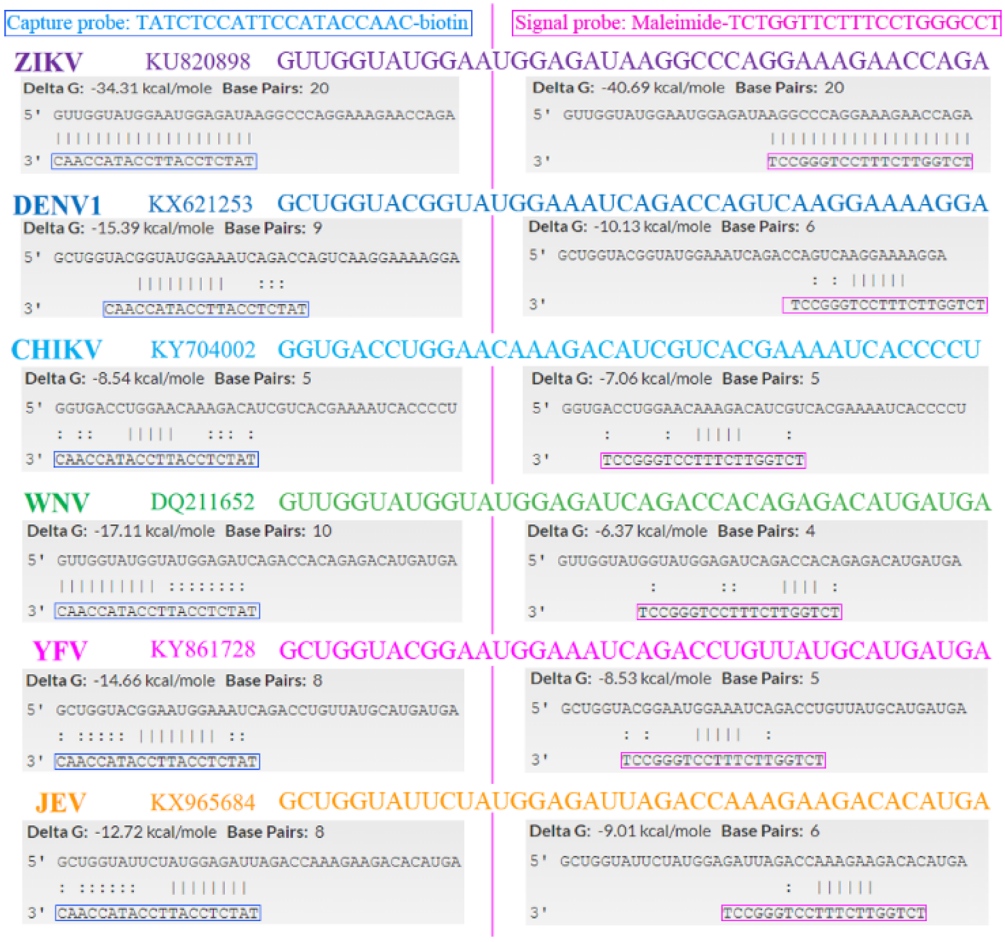

Figure 5. Sequence of ZIKV and other flavivirus strains, sequence of capture probe and signal probe, kinetic parameters, and hybrid structure.

(Table S2), kinetic parameters, and hybrid structure are shown in Figure 5.

With the designed sequence, we assessed the sensitivity and specificity of the dendritic $Ru(bpy)_3^{2+}$-polymer amplified ECL-scan imaging system for ZIKV. First, we verified the specificity of the dendritic $Ru(bpy)_3^{2+}$-polymer amplified ECL-scan imaging system with other flaviviruses. The results in Figure 6A indicated that the dendritic $Ru(bpy)_3^{2+}$-polymer amplified ECL-scan imaging system could specifically respond to ZIKV, and the other flavivirus group did not give out the ECL signal that could be differentiated from the control group. Therefore, the specificity of dendritic $Ru(bpy)_3^{2+}$-polymer amplified ECL-scan imaging system obtained a better proof. The sensitivity was also evaluated in Figure 6A, and the results of low concentration were shown in Figure S7. The results revealed that dendritic $Ru(bpy)_3^{2+}$-polymer amplified ECL-scan imaging system reached a satisfactory sensitivity of 50 copies for the ZIKV samples, which is higher for conventional methods including reverse transcription (RT)-PCR (100 copies), nucleic acid sequence-based amplification (NASBA) (100 copies), and ELISA (10−30 ng/mL).

Subsequently, the blood and urine samples from the ZIKV infected mouse mode were collected and detected. The blood samples and urine samples were treated by SDS buffer by five times' the volume. The blood sample from the mouse that infected the ZIKV was first detected. The results in Figure 6B revealed that the dendritic $Ru(bpy)_3^{2+}$-polymer amplified ECL-scan imaging system achieved a stable signal of the detection process. The urine sample from the infected mouse was collected by a simple device reported by our group. The results in Figure 6C indicated that the dendritic $Ru(bpy)_3^{2+}$-polymer amplified ECL-scan imaging system could stably respond to all the ZIKV samples from the urine of infected mouse. Furthermore, the spiked samples in human blood and urine was detected to verify the feasibility for ZIKV detection in human samples. The results in Figure 6D to F (spiked blood samples) and Figure 6G to I (spiked urine samples) proved the capacity of dendritic $Ru(bpy)_3^{2+}$-polymer amplified ECL-scan imaging system for the detection of human samples. Thus, it can be proven that this dendritic $Ru(bpy)_3^{2+}$-polymer amplified ECL-scan imaging system possesses the ability to detect ZIKV from complex environments.

Application of Dendritic $Ru(bpy)_3^{2+}$-Polymer Amplified ECL-Scan Imaging System for SARS-Cov2. The COVID-19 spread globally and caused immeasurable damages. More than six million patients were confirmed to be infected with SARS-Cov2 until Jun-4-2020. The high mortality brought unprecedented influence on human society. Thus, the monitoring of a highly pathogenic virus is of great significance to the prevention and control of emerging infectious diseases. In this section, the sequence of S protein and N protein gene were chosen as the instances for detection of SARS-Cov2 with the dendritic $Ru(bpy)_3^{2+}$-polymer amplified ECL-scan imaging system. The selected sequence of S protein and N protein gene, the capture and signal probe (Table S3), kinetic parameters, and hybrid structure were listed in Figure 7A.

https://doi.org/10.1021/acsomega.2c04280
ACS Omega 2022, 7, 37499−37508

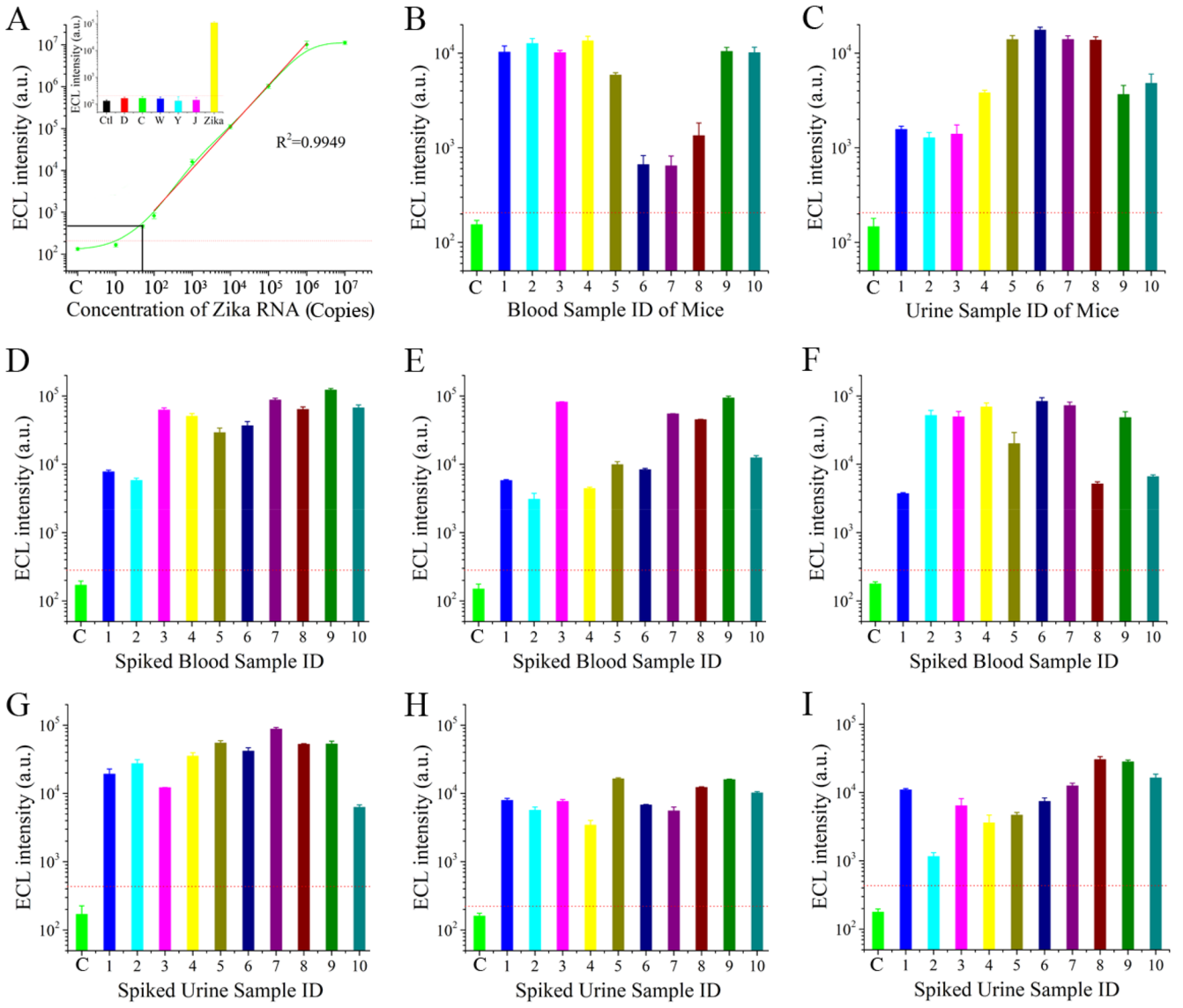

Figure 6. Performance Evaluation of Dendritic $Ru(bpy)_3^{2+}$-Polymer Amplified ECL-scan Imaging System for ZIKV. (A) Sensitivity and specificity of dendritic $Ru(bpy)_3^{2+}$-polymer amplified ECL-scan imaging system for ZIKV. (B) Detection of blood samples of mice. (C) Detection of urine samples of mice. (D to F) Detection of ZIKV spiked human blood samples. (G to I) Detection of ZIKV spiked human urine samples.

With the synthetic sequence, we examined the sensitivity and specificity of the dendritic $Ru(bpy)_3^{2+}$-polymer amplified ECL-scan imaging system for SARS-Cov2. The results in Figure 7B,C indicated that dendritic $Ru(bpy)_3^{2+}$-polymer amplified ECL-scan imaging system achieved a consistent performance with ZIKV detection. The sensitivity of 10 copies and preferable specificity were achieved with the spiked pseudovirus samples, and the results of low concentration were shown in Figures S8 and S9. The detection of spiked saliva and blood samples also confirmed the outstanding capacity of dendritic $Ru(bpy)_3^{2+}$-polymer amplified ECL-scan imaging system for detection in human samples.

CONCLUSIONS

A dendritic polymer probe-amplified ECL-scan imaging system was constructed to realize trace analysis of a viral emerging infectious disease. A dendritic polymer probe was employed as the efficient signal emitter component that could generate an amplified ECL signal on the integrated chip, and the signal was detected by a single-photon level charge coupled device-based ECL-scan imaging system. With this strategy, the ZIKV in the complex system of blood, urine, and saliva was detected. The results indicated that a high sensitivity of 50 copies and superior specificity were achieved. Furthermore, this strategy simultaneously realized highly sensitive detection (10 copies) of the S protein gene sequence of Severe Acute Respiratory Syndrome Coronavirus 2 (SARS-Cov2) and spiked samples. Therefore, the dendritic polymer probe-amplified ECL-scan imaging system suitably met the strict clinical requirements for trace analysis of highly pathogenic viruses, and thus has the potential to serve as a liquid biopsy paradigm for monitoring viral emerging infectious diseases.

EXPERIMENTAL SECTION

Reagents. All the chemical reagents for the synthesis and activation of $Ru(bpy)_3^{2+}$, such as cis-bis (2,2′-bipyridine) dichlororuthenium(II), 2,2′-bipyridine-4,4′-dicarboxylic acid, *N*,*N*′-dicyclohexylcarbodiimide (DCC), sodium hexafluoro-

https://doi.org/10.1021/acsomega.2c04280
ACS Omega 2022, 7, 37499−37508

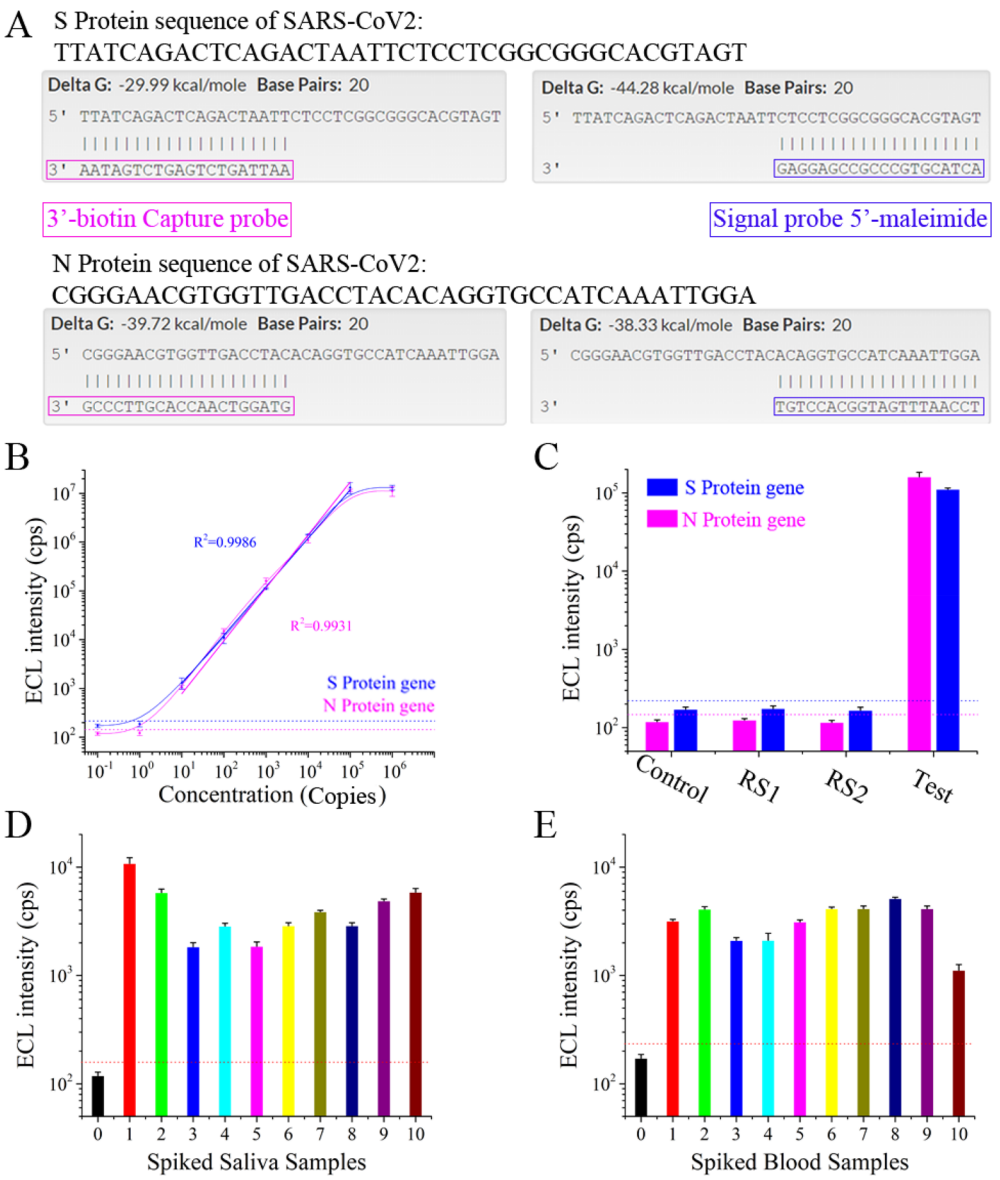

Figure 7. Performance evaluation of dendritic $Ru(bpy)_3^{2+}$-polymer amplified ECL-scan imaging system for SARS-Cov2. (A) Selected sequence of S protein and N protein gene, the capture and signal probe, kinetic parameters, and hybrid structure. (B) Sensitivity of dendritic $Ru(bpy)_3^{2+}$-polymer amplified ECL-scan imaging system for SARS-Cov2. (C) Specificity of dendritic $Ru(bpy)_3^{2+}$-polymer amplified ECL-scan imaging system for SARS-Cov2. (D) Detection of spiked saliva samples. (E) Detection of spiked blood samples.

phosphate, *N*-(3-(dimethylamino)propyl)-*N*′-ethylcarbodiimide hydrochloride (EDC), *N*-hydroxysuccinimide (NHS), and sodium borate were obtained from Alfa Aesar Co., Ltd. The single-photon level charge coupled device was customized by Tucsen Photonics Co., Ltd. Streptavidin magnetic beads were synthesized by New England BioLabs. Reagents related to electrophoresis and DNA probes were purchased from Shanghai Sangon Biotechnology Co. Ltd. SYBR I and SYBR II were purchased from APExBIO (Houston, USA). Reagent grade dendritic polymer was purchased from Sigma-Aldrich and was used without further purification except where noted. Invitrogen synthesized all oligonucleotides. Glass botttom dishes and centrifuge tubes were obtained from NEST Biotechnology (Wuxi, China).

Synthetic Routes of $Ru(bpy)_3^{2+}$. The synthesis routes of active $Ru(bpy)_3^{2+}$ followed the procedure of $Ru(bpy)_2(dcbpy)(PF_6)_2$ and the activation step of the carboxyl on $Ru(bpy)_3^{2+}$. The protocols were based on the previous works.[47,48] The detailed synthetic routes of $Ru(bpy)_3^{2+}$ are shown in Figure S2. The reactant of cis-dichlorobis(2,2′-bipyridine)ruthenium(II) with an excess of the corresponding 2,2′-bipyridine-4,4′-dicarboxylic acid (1:1.2) was refluxed in an ethanol/water (80%) mixture, and the mixture was incubated at 80 °C for one night to synthesize $Ru(bpy)_2(dcbpy)(PF_6)_2$. Then, the solution was subsequently cooled and acidified (pH = 4.4) to crystallize out the unreacted 2,2′-bipyridine-4,4′-dicarboxylic acid, which was eliminated by a qualitative filter paper based suction filter. The precooled solution of sodium hexafluorophosphate ($NaPF_6$) was added to the resultant filtrate, isolating the ruthenium complexes as PF_6 salts. The mixture was cooled with an ice−water mixture. Then, the crystal products were treated with the freeze-drying process to eliminate the influence of volatile solvent.

https://doi.org/10.1021/acsomega.2c04280
ACS Omega 2022, 7, 37499−37508

Synthetic Routes of Dendric Ru(bpy)$_3^{2+}$-Polymer. The core of dendric polymer was obtained from Sigma, then modified with amino via the lipid reaction. The mixture of maleimide-labeled DNA and the amino-labeled dendric polymer (the molecular ratio between maleimide-labeled DNA and the amino-labeled dendric polymer was set as 20:1) was incubated for 12 h at 37 °C with stirring. Then, the dissociative DNA was eliminated by ultrafiltration to increase the sensitivity and signal-to-noise ratio. The purified products were mixed with carboxyl-activated Ru(bpy)$_3^{2+}$ at the molecular ratio of 1:5000, and incubated at 37 °C for 12 h with stirring. The products were purified by ultrafiltration to eliminate free Ru(bpy)$_3^{2+}$.

Dissociation Process of Virus. The virus samples were cracked by a commercial virus-lysis kit, the key constituent was sodium dodecyl sulfate (SDS), and the solution was heated to 60 °C for 5 min. Then, 10 μL of magnetic beads (1 mg/mL) labeled with the capture probe was added in each sample for 10 min. The mixture was processed by magnetic separation. The captured products were collected for later ECL steps.

ECL Process. The signal probe, composed of the dendric Ru(bpy)$_3^{2+}$-polymer and DNA recognition domain, was employed as the ECL-generating group. The signal probe and NHS-activated dendric Ru(bpy)$_3^{2+}$-polymer were incubated at room temperature (R.T.) in a 1:1 molar ratio for covalent linkage. Meanwhile, the biotin labeled capture probes (10 μM) were bound to the magnetic beads (10^4/mL) labeled with the streptavidin through R.T. co-incubation. Then the sample containing target nucleic acid was added into the excess mixture of signal probe-dendric Ru(bpy)$_3^{2+}$-polymer and capture probe-magnetic beads (the molar ratio of the signal probe and the capture probe was 1:1) for specific binding, and the classical "sandwich" structure of ECL was constituted. A gradient cooling process would be more effective for formation. After the cleaning steps by magnetic bead adsorption and PBS washing for 4 times, the ECL signal of the "sandwich" structure was detected in the presence of the coreactant of tripropylamine (TPA, 10 μM). Typically, the electrode voltage and the accepted wavelength range of the ECL instrument was set as 2.4 V, and 300−800 nm, respectively. The parameters such as exposure time, effective area, pixel size, and resolution of the CCD system was set as 12 s, 11.1 × 6.3 mm^2, 2.9 μm (H) × 2.9 μm (V), and 3840 (H) × 2160 (V), respectively.

■ ASSOCIATED CONTENT

Supporting Information

The Supporting Information is available free of charge at https://pubs.acs.org/doi/10.1021/acsomega.2c04280.

Principle of probe assembly; synthetic routes of Ru(bpy)$_3^{2+}$; stability of dendritic Ru(bpy)$_3^{2+}$-polymer probe; result details of low concentration samples; sequence of target RNA and probes (PDF)

■ AUTHOR INFORMATION

Corresponding Authors

Yuhui Liao − *Molecular Diagnosis and Treatment Center for Infectious Diseases, Dermatology Hospital of Southern Medical University, Guangzhou 510091, China; Department of Infectious Disease, Fifth Affiliated Hospital of Sun Yat-sen University, Zhuhai 519000, China;* orcid.org/0000-0003-4702-9516; Email: liaoyh8@mail.sysu.edu.cn

Xiaodong Chen − *Department of Burn Surgery & Department of Clinical Laboratory, First People's Hospital of Foshan, Foshan 528000, China*; Email: cxd234@163.com

Jinyu Xia − *Department of Infectious Disease, Fifth Affiliated Hospital of Sun Yat-sen University, Zhuhai 519000, China*; Email: xiajinyu@mail.sysu.edu.cn

Baoqing Sun − *Guangzhou Institute of Respiratory Health, State Key Laboratory of Respiratory Disease, National Clinical Research Center of Respiratory Disease, First Affiliated Hospital of Guangzhou Medical University, Guangzhou 510120, China*; Email: sunbaoqing@vip.163.com

Authors

Yunxia Wu − *Department of Burn Surgery & Department of Clinical Laboratory, First People's Hospital of Foshan, Foshan 528000, China*

Ronghua Yang − *Department of Burn and Plastic Surgery, Guangzhou First People's Hospital, Guangzhou 510180, China*

Qikang Wu − *Department of Burn Surgery & Department of Clinical Laboratory, First People's Hospital of Foshan, Foshan 528000, China*

Mingxing Huang − *Department of Infectious Disease, Fifth Affiliated Hospital of Sun Yat-sen University, Zhuhai 519000, China*

Bowen Shu − *Molecular Diagnosis and Treatment Center for Infectious Diseases, Dermatology Hospital of Southern Medical University, Guangzhou 510091, China*

Wenjie Wu − *Molecular Diagnosis and Treatment Center for Infectious Diseases, Dermatology Hospital of Southern Medical University, Guangzhou 510091, China*

Complete contact information is available at: https://pubs.acs.org/10.1021/acsomega.2c04280

Author Contributions

#Y.W., R.Y., Q.W., and M.H. contributed equally.

Notes

The authors declare no competing financial interest.

■ ACKNOWLEDGMENTS

This work was supported by the National Key R&D Program of China (2021YFC2302200), Natural Science Fund of Guangdong Province for Distinguished Young Scholars (22050000282), National Natural Science Foundation of China (81972019, 21904145, 82102360, 81772136), Special Fund of Foshan Summit Plan (2020B019, 2020B012, 2020A015), Zhongnanshan Medical Foundation of Guangdong Province (ZNSA-2021012), Training project of National Science Foundation for Outstanding/Distinguished Young Scholars of Southern Medical University (C620PF0217), China Postdoctoral Science Foundation (2021M690634), Guangdong Basic and Applied Basic Research Foundation (2020A1515110529), Foundation of Foshan City (FS0AA-KJ218-1301-0034, 2018AB003411), Guangzhou Institute of Respiratory Health Open Project (Funds provided by China Evergrande Group, Project No. 2020GIRHHMS04).

■ REFERENCES

(1) Petersen, L. R.; Jamieson, D. J.; Powers, A. M.; Honein, M. A. Zika virus. *N. Engl. J. Med.* **2016**, *374*, 1552−1563.

(2) Mlakar, J.; Korva, M.; Tul, N.; Popović, M.; Poljšak-Prijatelj, M.; Mraz, J.; Kolenc, M.; Resman Rus, K.; Vesnaver Vipotnik, T.; Fabjan

Vodušek, V. Zika virus associated with microcephaly. *N. Engl. J. Med.* **2016**, *374*, 951−958.
(3) Baud, D.; Gubler, D. J.; Schaub, B.; Lanteri, M. C.; Musso, D. An update on Zika virus infection. *Lancet* **2017**, *390*, 2099−2109.
(4) Du, S.; Liu, Y.; Liu, J.; Zhao, J.; Champagne, C.; Tong, L.; Zhang, R.; Zhang, F.; Qin, C.-F.; Ma, P.; et al. Aedes mosquitoes acquire and transmit Zika virus by breeding in contaminated aquatic environments. *Nat. Commun.* **2019**, *10*, 1−11.
(5) Gutiérrez-Bugallo, G.; Piedra, L. A.; Rodriguez, M.; Bisset, J. A.; Lourenço-de-Oliveira, R.; Weaver, S. C.; Vasilakis, N.; Vega-Rúa, A. Vector-borne transmission and evolution of Zika virus. *Nature ecology & evolution* **2019**, *3*, 561−569.
(6) Fauci, A. S.; Morens, D. M. Zika virus in the Americas-yet another arbovirus threat. *N. Engl. J. Med.* **2016**, *374*, 601−604.
(7) Faria, N. R.; da Silva Azevedo, R. d. S.; Kraemer, M. U.; Souza, R.; Cunha, M. S.; Hill, S. C.; Thézé, J.; Bonsall, M. B.; Bowden, T. A.; Rissanen, I.; et al. Zika virus in the Americas: early epidemiological and genetic findings. *Science* **2016**, *352*, 345−349.
(8) Zhang, Q.; Sun, K.; Chinazzi, M.; y Piontti, A. P.; Dean, N. E.; Rojas, D. P.; Merler, S.; Mistry, D.; Poletti, P.; Rossi, L. Spread of Zika virus in the Americas. *Proc. Natl. Acad. Sci. U. S. A.* **2017**, *114*, E4334−E4343.
(9) Roos, R. P. Zika virus-a public health emergency of international concern. *JAMA Neurol.* **2016**, *73*, 1395−1396.
(10) Gulland, A. Zika virus is a global public health emergency, declares WHO. *Br. Med. J.* **2016**, *352*, i657.
(11) Maurice, J. The Zika virus public health emergency: 6 months on. *Lancet* **2016**, *388*, 449−450.
(12) Martínez-Rojas, P. P.; Quiroz-García, E.; Monroy-Martínez, V.; Agredano-Moreno, L. T.; Jiménez-García, L. F.; Ruiz-Ordaz, B. H. Participation of Extracellular Vesicles from Zika-Virus-Infected Mosquito Cells in the Modification of Naïve Cells' Behavior by Mediating Cell-to-Cell Transmission of Viral Elements. *Cells* **2020**, *9*, 123.
(13) Liu, Y.; Liu, J.; Du, S.; Shan, C.; Nie, K.; Zhang, R.; Li, X. F.; Zhang, R.; Wang, T.; Qin, C. F.; et al. Evolutionary enhancement of Zika virus infectivity in Aedes aegypti mosquitoes. *Nature* **2017**, *545*, 482−486.
(14) Quicke, K. M.; Bowen, J. R.; Johnson, E. L.; McDonald, C. E.; Ma, H.; O'Neal, J. T.; Rajakumar, A.; Wrammert, J.; Rimawi, B. H.; Pulendran, B.; et al. Zika virus infects human placental macrophages. *Cell Host Microbe* **2016**, *20*, 83−90.
(15) McCarthy, M. Zika virus was transmitted by sexual contact in Texas, health officials report. *Br. Med. J.* **2016**, *352*, i720.
(16) D'Ortenzio, E.; Matheron, S.; de Lamballerie, X.; Hubert, B.; Piorkowski, G.; Maquart, M.; Descamps, D.; Damond, F.; Yazdanpanah, Y.; Leparc-Goffart, I. Evidence of sexual transmission of Zika virus. *N. Engl. J. Med.* **2016**, *374*, 2195−2198.
(17) Musso, D.; Stramer, S. L.; Busch, M. P. Zika virus: a new challenge for blood transfusion. *Lancet* **2016**, *387*, 1993−1994.
(18) Cao-Lormeau, V. M.; Blake, A.; Mons, S.; Lastère, S.; Roche, C.; Vanhomwegen, J.; Dub, T.; Baudouin, L.; Teissier, A.; Larre, P.; et al. Guillain-Barré Syndrome outbreak associated with Zika virus infection in French Polynesia: a case-control study. *Lancet* **2016**, *387*, 1531−1539.
(19) Parra, B.; Lizarazo, J.; Jiménez-Arango, J. A.; Zea-Vera, A. F.; González-Manrique, G.; Vargas, J.; Angarita, J. A.; Zuñiga, G.; Lopez-Gonzalez, R.; Beltran, C. L.; et al. Guillain-Barré syndrome associated with Zika virus infection in Colombia. *N. Engl. J. Med.* **2016**, *375*, 1513−1523.
(20) Li, C.; Xu, D.; Ye, Q.; Hong, S.; Jiang, Y.; Liu, X.; Zhang, N.; Shi, L.; Qin, C. F.; Xu, Z. Zika virus disrupts neural progenitor development and leads to microcephaly in mice. *Cell stem cell* **2016**, *19*, 120−126.
(21) Russo, F. B.; Jungmann, P.; Beltrão-Braga, P. C. B. Zika infection and the development of neurological defects. *Cell. Microbiol.* **2017**, *19*, No. e12744.
(22) Guan, W. J.; Ni, Z. Y.; Hu, Y.; Liang, W. H.; Ou, C. Q.; He, J. X.; Liu, L.; Shan, H.; Lei, C. L.; Hui, D. S.; et al. Clinical characteristics of coronavirus disease 2019 in China. *N. Engl. J. Med.* **2020**, *382*, 1708−1720.
(23) World Health Organization. *Protocol for assessment of potential risk factors for coronavirus disease 2019 (COVID-19) among health workers in a health care setting, 23 March 2020*; World Health Organization: 2020.
(24) Mehta, P.; McAuley, D. F; Brown, M.; Sanchez, E.; Tattersall, R. S; Manson, J. J COVID-19: consider cytokine storm syndromes and immunosuppression. *Lancet* **2020**, *395*, 1033−1034.
(25) Praticò, A. D. COVID-19 pandemic for Pediatric Health Care: disadvantages and opportunities. *Pediatr. Res.* **2020**, 709.
(26) Greenhalgh, T.; Koh, G. C. H.; Car, J. Covid-19: a remote assessment in primary care. *Br. Med. J.* **2020**, *368*, m1182.
(27) Liao, M.; Liu, Y.; Yuan, J.; Wen, Y.; Xu, G.; Zhao, J.; Cheng, L.; Li, J.; Wang, X.; Wang, F.; Liu, L.; Amit, I.; Zhang, S.; Zhang, Z. Single-cell landscape of bronchoalveolar immune cells in patients with COVID-19. *Nat. Med.* **2020**, *26*, 842.
(28) Cao, X. COVID-19: immunopathology and its implications for therapy. *Nat. Rev. Immunol.* **2020**, *20*, 269−270.
(29) Greenhalgh, T.; Koh, G. C. H.; Car, J. Covid-19: a remote assessment in primary care. *Br. Med. J.* **2020**, *368*, m1182.
(30) Monteil, V.; Kwon, H.; Prado, P.; Hagelkrüys, A.; Wimmer, R. A.; Stahl, M.; Leopoldi, A.; Garreta, E.; Del Pozo, C. H.; Prosper, F.; et al. Inhibition of SARS-CoV-2 infections in engineered human tissues using clinical-grade soluble human ACE2. *Cell* **2020**, *181*, 905−913.
(31) Kraemer, M. U. G.; Yang, C. H.; Gutierrez, B.; Wu, C. H.; Klein, B.; Pigott, D. M.; du Plessis, L.; Faria, N. R.; Li, R.; Hanage, W. P.; Brownstein, J. S.; Layan, M.; Vespignani, A.; Tian, H.; Dye, C.; Pybus, O. G.; Scarpino, S. V. The effect of human mobility and control measures on the COVID-19 epidemic in China. *Science* **2020**, *368*, 493−497.
(32) Yockey, L. J.; Lucas, C.; Iwasaki, A. Contributions of maternal and fetal antiviral immunity in congenital disease. *Science* **2020**, *368*, 608−612.
(33) Baud, D.; Qi, X.; Nielsen-Saines, K.; Musso, D.; Pomar, L.; Favre, G. Real estimates of mortality following COVID-19 infection. *Lancet Infect. Dis.* **2020**, *20*, 773.
(34) Yuan, J.; Li, M.; Lv, G.; Lu, Z. K. Monitoring transmissibility and mortality of COVID-19 in Europe. *Int. J. Infect. Dis.* **2020**, *95*, 311−315.
(35) Mahase, E. Covid-19: UK starts social distancing after new model points to 260 000 potential deaths. *Br. Med. J.* **2020**, *368*, m1089.
(36) Remuzzi, A.; Remuzzi, G. COVID-19 and Italy: what next? *Lancet* **2020**, *395*, 1225−1228.
(37) Lazzerini, M.; Putoto, G. COVID-19 in Italy: momentous decisions and many uncertainties. *Lancet Global Health* **2020**, *8*, E641−E642.
(38) Vinyard, D. J.; Su, S.; Richter, M. M. Electrogenerated chemiluminescence of 9,10-diphenylanthracene, rubrene, and anthracene in fluorinated aromatic solvents. *J. Phys. Chem. A* **2008**, *112*, 8529−8533.
(39) Vasilopoulou, M.; Mohd Yusoff, A. R. B.; Daboczi, M.; Conforto, J.; Gavim, A. E. X.; da Silva, W. J.; Macedo, A. G.; Soultati, A.; Pistolis, G.; Schneider, F. K.; Dong, Y.; Jacoutot, P.; Rotas, G.; Jang, J.; Vougioukalakis, G. C.; Chochos, C. L.; Kim, J. S.; Gasparini, N. High efficiency blue organic light-emitting diodes with below-bandgap electroluminescence. *Nat. Commun.* **2021**, *12*, 4868.
(40) Rhyne, P. W.; Wong, O. T.; Zhang, Y. J.; Weiner, R. S. Electrochemiluminescence in bioanalysis. *Bioanal.* **2009**, *1*, 919−935.
(41) Forster, R. J.; Bertoncello, P.; Keyes, T. E. Electrogenerated chemiluminescence. *Annu. Rev. Anal. Chem.* **2009**, *2*, 359−385.
(42) Hiramoto, K.; Villani, E.; Iwama, T.; Komatsu, K.; Inagi, S.; Inoue, K. Y.; Nashimoto, Y.; Ino, K.; Shiku, H. Recent Advances in Electrochemiluminescence-Based Systems for Mammalian Cell Analysis. *Micromachines* **2020**, *11*, 530−539.

https://doi.org/10.1021/acsomega.2c04280
ACS Omega 2022, 7, 37499−37508

(43) Muzyka, K.; Saqib, M.; Liu, Z.; Zhang, W.; Xu, G. Progress and challenges in electrochemiluminescent aptasensors. *Biosens. Bioelectron.* **2017**, *92*, 241−258.
(44) Miao, W. Electrogenerated chemiluminescence and its biorelated applications. *Chem. Rev.* **2008**, *108*, 2506−2553.
(45) Richter, M. M. Electrochemiluminescence (ECL). *Chem. Rev.* **2004**, *104*, 3003−3036.
(46) Liao, Y.; Fan, Z.; Deng, H.; Yang, Y.; Lin, J.; Zhao, Z.; Tan, Q.; Li, B.; Huang, X. Zika Virus Liquid Biopsy: A Dendritic Ru $(bpy)_3^{2+}$-Polymer-Amplified ECL Diagnosis Strategy Using a Drop of Blood. *ACS Cent. Sci.* **2018**, *4*, 1403−1411.
(47) Liao, Y.; Zhou, X.; Fu, Y.; Xing, D. Linear Ru $(bpy)_3^{2+}$-polymer as a universal probe for sensitive detection of biomarkers with controllable electrochemiluminescence signal-amplifying ratio. *Anal. Chem.* **2017**, *89*, 13016−13023.
(48) Zhao, Z.; Tan, Q.; Zhan, X.; Lin, J.; Fan, Z.; Xiao, K.; Li, B.; Liao, Y.; Huang, X. Cascaded Electrochemiluminescence Signal Amplifier for the Detection of Telomerase Activity from Tumor Cells and Tissues. *Theranostics* **2018**, *8*, 5625−5633.

https://doi.org/10.1021/acsomega.2c04280
ACS Omega 2022, 7, 37499−37508